Second Harmonic Generation

International Edition: DOI: 10.1002/anie.201606782
German Edition: DOI: 10.1002/ange.201606782

Pb_2BO_3Cl: A Tailor-Made Polar Lead Borate Chloride with Very Strong Second Harmonic Generation

*Guohong Zou, Chensheng Lin, Hongil Jo, Gnu Nam, Tae-Soo You, and Kang Min Ok**

Abstract: *A meticulously designed, polar, non-centrosymmetric lead borate chloride, Pb_2BO_3Cl, was synthesized using $KBe_2BO_3F_2$ (KBBF) as a model. Single-crystal X-ray diffraction revealed that the structure of Pb_2BO_3Cl consists of cationic $[Pb_2(BO_3)]^+$ honeycomb layers and Cl^- anions. Powder second harmonic generation (SHG) measurements on graded polycrystalline Pb_2BO_3Cl indicated that the title compound is phase-matchable (type I) and exhibits a remarkably strong SHG response, which is approximately nine times stronger than that of potassium dihydrogen phosphate, and the largest efficiency observed in materials with structures similar to KBBF. Further characterization suggested that the compound melts congruently at high temperature and has a wide transparency window from the near-UV to the mid-IR region.*

Nonlinear optical (NLO) materials,[1] the key components of solid-state lasers producing coherent light through a cascaded frequency conversion, have received extensive commercial and academic interest owing to their versatile scientific and technological applications. Over the past several decades, many efforts have been devoted to elucidating the relationship of the structures, compositions, and NLO properties of crystalline compounds; however, it still remains challenging to efficiently design novel NLO materials with excellent overall properties, including large second harmonic generation (SHG) coefficients, moderate birefringence for the phase-matching condition, wide transparency windows for a high damage threshold, good chemical stability, and facile crystal growth.

A few strategies for creating new NLO materials employ non-centrosymmetric (NCS) chromophores, such as anions in π-delocalized systems,[1b,2] second-order Jahn–Teller (SOJT) distorted cations (d^0 cations exhibiting intra-octahedral distortion and cations with stereochemically active lone pairs),[2f,3] and d^{10} metal cations with polar displacement,[4] as building units during the syntheses. Metal borates have been intensively investigated as ultraviolet (UV) or deep-UV NLO materials. Developing NLO crystals based on borate systems has been particularly successful on the basis of anionic group theory,[5] where the overall crystal non-linearity is the geometrical superposition of the microscopic second-order susceptibility of the NLO-active anionic groups.[6] Thus far, a variety of important UV NLO crystals, including β-BaB_2O_4 (BBO),[7] LiB_3O_5 (LBO),[8] CsB_3O_5 (CBO),[9] $CsLiB_6O_{10}$ (CLBO),[10] and $YCa_4O(BO_3)_3$ (YCOB),[11] have been discovered. The discovery of $KBe_2BO_3F_2$ (KBBF) was a breakthrough in the area of deep-UV NLO crystals[12] as it is the only material that can generate coherent light at wavelengths below 200 nm by direct SHG. The excellent NLO properties of KBBF, such as moderate SHG coefficients, a wide transparency window, and proper birefringence, certainly arise from its distinct crystal structure. The $[Be_2BO_3F_2]_\infty$ layers made up from tetrahedral $[BeO_3F]$ units and the trigonal-planar $[BO_3]$ units within the chiral structure adopt a coplanar configuration to promote SHG and birefringence. The firm linkages between the three terminal oxygen atoms of the BO_3 groups and the Be atoms prevent the formation of dangling bonds in the BO_3 groups, which results in a very short absorption edge in the UV region.

Owing to the structure-based superior NLO properties of KBBF, many researchers have made long-lasting endeavors to develop similarly excellent new NLO crystals. A few representative compounds belonging to the KBBF family are $ABe_2B_3O_7$ (A = K or Rb),[13] $Na_2CsBe_6B_5O_{15}$,[14] $NaSr_3Be_3B_3O_9F_4$,[15] $NaCaBe_2B_2O_6F$,[16] and $Cs_3Zn_6B_9O_{21}$.[17] In spite of their distinguished characteristics, it is very difficult to grow large crystals of the KBBF family owing to their layered structures. With these ideas in mind, we utilized a tailored molecular design approach by selectively modifying the KBBF structure to develop an excellent UV NLO material based on Pb, B, O, and Cl. First, replacement of the alkaline-earth-metal cation, Be^{2+}, in the $[Be_2BO_3F_2]^-_\infty$ layers by the lone-pair cation Pb^{2+} was expected to lead to large birefringence and an enhanced SHG response owing to the strong electronic polarizability as well as the stereoactive lone pair.[18] Second, the F atom in the tetrahedral $[PbO_3F]$ unit was removed to make room between the layers so that the lone pairs in the $[PbO_3]$ units remain stereoactive. Third, a light halide, Cl^-, was introduced for charge balance as well as to cause an effective blue shift of the UV absorption edge. Guided by these ideas, we were able to synthesize a novel congruently melting NLO material, Pb_2BO_3Cl, which consists of the targeted $[Pb_2BO_3]^+_\infty$ layers and Cl^- anions. Powder NLO measurements indicate that Pb_2BO_3Cl exhibits the largest SHG response in the KBBF family, which is approx-

[*] Dr. G. Zou, H. Jo, Prof. Dr. K. M. Ok
Department of Chemistry, Chung-Ang University
Seoul 06974 (Republic of Korea)
E-mail: kmok@cau.ac.kr
Dr. C. Lin
Fujian Institute of Research on the Structure of Matter
Chinese Academy of Sciences
Fuzhou, Fujian 350002 (China)
G. Nam, Prof. Dr. T.-S. You
Department of Chemistry, Chungbuk National University
Cheongju, Chungbuk 28644 (Republic of Korea)
Supporting information and the ORCID identification number(s) for the author(s) of this article can be found under: http://dx.doi.org/10.1002/anie.201606782.

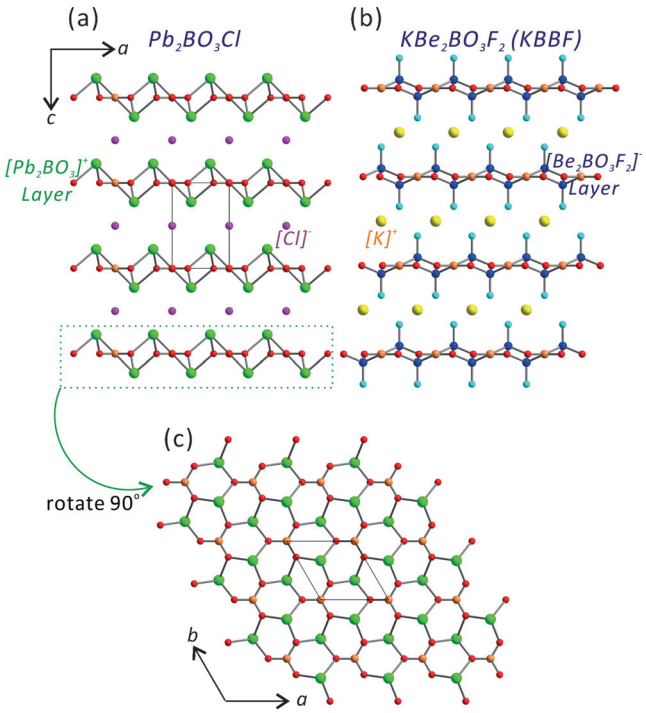

Figure 1. Ball-and-stick models of a) Pb_2BO_3Cl and b) $KBe_2BO_3F_2$ (KBBF) in the *ac* plane. B orange, Be blue, Cl purple, F cyan, K yellow, O red, Pb green. c) Each BO_3 planar triangle shares its corners with six PbO_3 trigonal pyramids and forms a honeycomb-like cationic $[Pb_2BO_3]^+$ layer in the *ab* plane of Pb_2BO_3Cl.

imately nine times stronger than that of potassium dihydrogen phosphate (KDP).

Pb_2BO_3Cl crystallizes in the trigonal polar NCS space group *P*321 (No. 150). As shown in Figure 1a, the structure of Pb_2BO_3Cl is composed of cationic $[Pb_2BO_3]^+$ layers made from BO_3 triangular units and PbO_3 trigonal pyramids with Cl^- anions residing in the interlayer space. As a new member of the KBBF family, Pb_2BO_3Cl can also be written as $[Cl]^-[Pb_2BO_3]^+$, with a structure comparable to that of $[K]^+[Be_2BO_3F_2]^-$ (see Figure 1b). Specifically, the $[Cl]^-$ anions occupy the positions of the $[K]^+$ cations in the interlayer space of KBBF for charge balance. The lone pairs on the Pb^{2+} cations in the cationic $[Pb_2BO_3]^+$ layer can somehow be considered as taking the place of the F^- anions in the anionic $[Be_2BO_3F_2]^-$ layer of KBBF. Within the cationic $[Pb_2BO_3]^+$ layer of Pb_2BO_3Cl, a unique B^{3+} cation is coordinated to three O atoms in the BO_3 planar-triangular geometry with B–O bond lengths of 1.370(17) Å. The Pb^{2+} cation lying on the site of 3*m* symmetry is also bonded to three O atoms in a trigonal-pyramidal coordination environment with Pb–O bond lengths of 2.297(8) Å. As seen in Figure 1c, each BO_3 planar triangle shares its corners with six PbO_3 trigonal pyramids and forms a honeycomb-like cationic $[Pb_2BO_3]^+$ layer in the *ab* plane. As we will discuss in more detail later, the cooperative interactions of the polarizable lone pairs in the PbO_3 trigonal pyramids and all the parallel triangular BO_3 groups oriented in the same direction within the layer may be mainly responsible for the large macroscopic SHG effect. The three dangling bonds of the BO_3 groups are successfully eliminated by robust bonding between the three terminal O atoms of the BO_3 group and Pb, which should broaden its transparency window. The bond valence sums[19] for Pb^{2+} and B^{3+} in Pb_2BO_3Cl were calculated to be 2.15 and 3.00, respectively.

The thermal behavior of Pb_2BO_3Cl was investigated by thermogravimetric analysis (TGA), differential scanning calorimetry (DSC), and powder X-ray diffraction (PXRD). Whereas no substantial weight loss was observed up to 640 °C in the TGA curve, an endothermic peak was located at about 630 °C in the DSC curve, which is attributable to the melting of Pb_2BO_3Cl (Figure 2a). The slight weight loss observed in

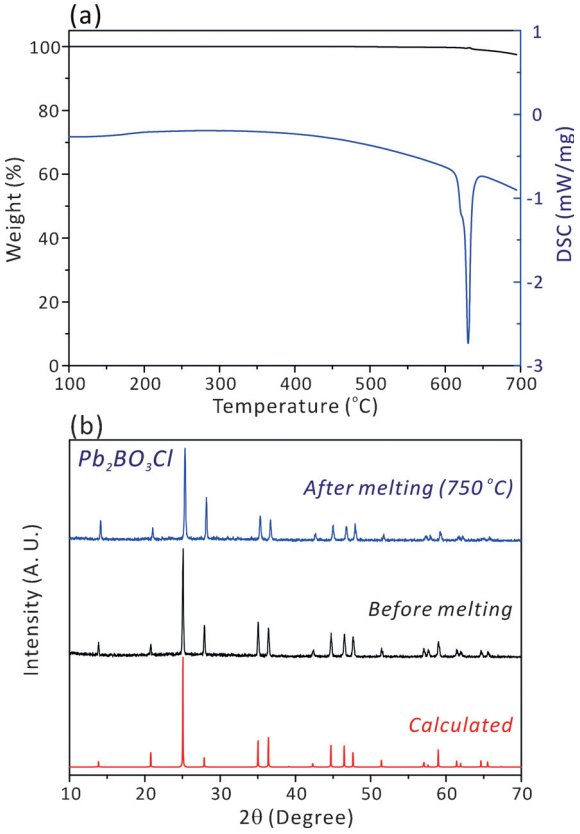

Figure 2. a) TGA and DSC analysis and b) calculated and experimental PXRD patterns for Pb_2BO_3Cl. Whereas no substantial weight loss was observed up to 640 °C in the TGA curve, an endothermic peak occurred at about 630 °C in the DSC curve, attributable to the melting of Pb_2BO_3Cl. The PXRD patterns for polycrystalline Pb_2BO_3Cl at room temperature and a sample heated to 750 °C were identical.

the TGA curve is possibly due to the volatility of Pb_2BO_3Cl at higher temperatures upon melting. In fact, the powder XRD patterns for polycrystalline Pb_2BO_3Cl measured at room temperature and a sample heated to 750 °C revealed identical patterns, which strongly suggests that Pb_2BO_3Cl melts congruently without any phase transitions (see Figure 2b). Thus large high-quality single crystals of Pb_2BO_3Cl could be grown by various crystal-growth methods.

The IR spectrum of Pb_2BO_3Cl revealed B–O and Pb–O vibrations. The broad bands observed at 1197 cm^{-1} were assigned to the B–O stretching vibrations. The strong bands at

742, 728, and 625 cm^{-1} were attributed to both the bending modes of the triangular BO_3 groups and the Pb–O stretching vibrations. The assignments are in agreement with other oxides containing B and Pb.[18c,20] The IR spectrum of Pb_2BO_3Cl is included in the Supporting Information.

A UV/Vis diffuse reflectance spectrum was also recorded for Pb_2BO_3Cl, and the absorption (K/S) data were calculated from the Kubelka–Munk function (Figure 3a).[21] As shown in Figure 3a, the UV absorption spectrum of Pb_2BO_3Cl exhibits

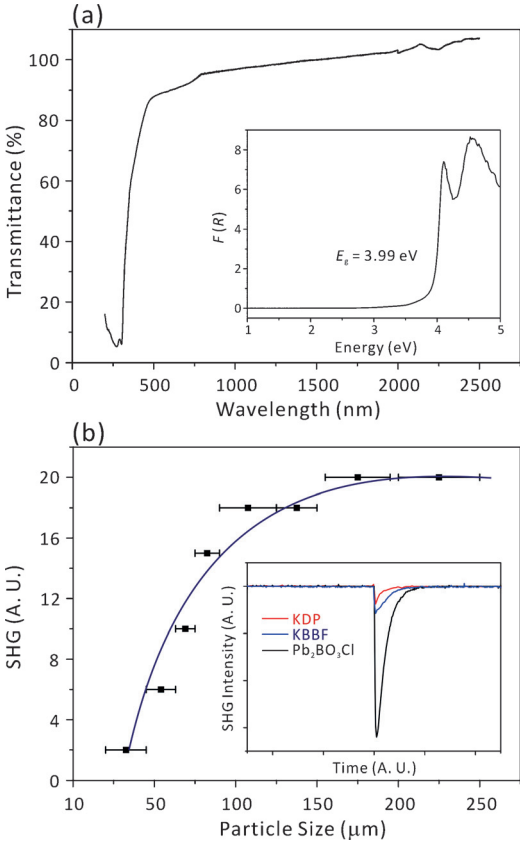

Figure 3. a) UV/Vis/NIR transmittance spectrum and b) phase-matching curve for Pb_2BO_3Cl. The curve is drawn as a guide to the eye and not a fit to the data. The insets in (a) and (b) are an optical diffuse reflectance spectrum and an oscilloscope trace showing the SHG intensity, respectively, for Pb_2BO_3Cl. The SHG intensities for KDP and KBBF are also plotted for comparison.

no absorption from 300 to 2500 nm, suggesting that the material has a wide transparency region ranging from the near-UV to the mid-IR. The observed UV absorption edge for Pb_2BO_3Cl is at a substantially shorter wavelength than those of other lead borates, which might be due to the light halide ion, Cl^-, that was introduced, which can effectively blue-shift the absorption edge. The diffuse reflectance spectrum also indicates that Pb_2BO_3Cl has a wide optical band gap of 3.99 eV.

Pb_2BO_3Cl exhibited a very large SHG response that was about nine times stronger than that of KDP and almost six times stronger than that of KBBF (see Figure 3b). Furthermore, the curve obtained by plotting the SHG signals as a function of the particle size determined for ground crystals of Pb_2BO_3Cl indicated that the material is type I phase-matchable (Figure 3b, inset).[1c,22]

To gain further insight into the band structure and optical properties of Pb_2BO_3Cl, density functional theory (DFT) calculations were performed by using the TB-LMTO-ASA method. The band-structure calculations predict a band gap of 2.32 eV for Pb_2BO_3Cl, which is considerably smaller than the experimental value (see Figure 4). It is well documented

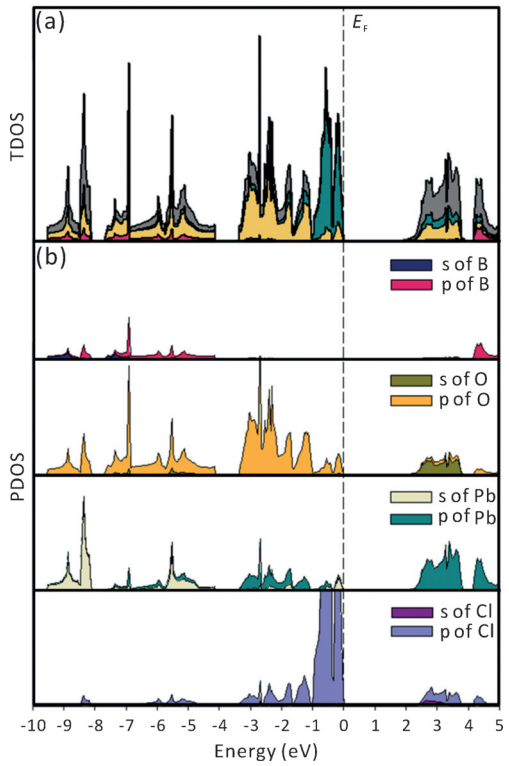

Figure 4. a) Total and b) partial DOS curves for Pb_2BO_3Cl. Individual PDOS curves of selected orbitals for B, O, Pb, and Cl are also shown. The E_F is displayed as a dashed vertical line and was used as a reference for all energy values (0 eV).

that electronic-band-structure calculations by DFT calculations tend to underestimate the energy gap.[23] However, the calculations are very helpful in locating the crucial orbital interactions. The total density of states (TDOS) curve shows an overall orbital mixing of four elements over the entire energy range as shown in Figure 4a. The valence band region below the Fermi level (E_F) can be divided into five smaller regions based on the atomic orbital contributions. In particular, the largest orbital contributions in the valence band region are due to the trigonal-planar-shaped $[BO_3]^{3-}$ moiety: 1) The lowest-energy region between −9.5 and −8 eV includes strong contributions from the s states of the central B atom and the p_y group orbitals of the surrounding three O atoms, leading to σ interactions with some mixing of Pb s states. 2) The region between −7.8 and −7 eV mostly displays the p_x and p_y states of B and the p_y group orbitals of three O atoms, which also contributes to the σ-interactions, with some contributions from the s states of Pb as well. 3) The

region between −7 and −4 eV contains large contributions from the p_z states of both B and the group orbitals of O, eventually building up the π interactions over the $[BO_3]^{3-}$ group. 4) The region between −3.5 and −1 eV contains rather small contributions from the p_x and p_y states of B and the large p_x states from the group orbitals of O, both of which form nearly non-bonding interactions between them, with some contributions from the p states of both Pb and Cl. 5) The region between −1 eV and E_F is mostly dominated by the p states of Cl. Interestingly, according to the partial DOS (PDOS) analyses for Pb and Cl, the s states of Pb somewhat contribute to regions 1 and 2, where the B and O atoms in the $[BO_3]^{3-}$ group form the σ interactions. In addition, the p states of Pb overlap with region 3, where the p_z states of both B and O lead to π interactions on the $[BO_3]^{3-}$ group. These interatomic interactions between Pb and O can be clearly observed in the Pb–O COHP curve shown in Figure S2. In addition, the p states of Cl also somewhat contribute to region 3, implying a particular interaction with orbitals of Pb as well (see Figure S2 b).

All of the interatomic interactions within the $[BO_3]^{3-}$ groups in the *ab* plane and among the $[BO_3]^{3-}$, Pb, and Cl units in the *ab* and *ac* planes can be clearly visualized by the electron localization function (ELF) diagrams (Figure 5 a). First, to look for interatomic interactions between the $[BO_3]^{3-}$ groups and Pb along the *ab* plane, we plotted (0 0 1) slices with $z = 0$ and $z = 0.112$ (Figure 5 a, b). In particular, in the (0 0 0.112) plane, which is located between 2D layers of $[BO_3]^{3-}$ and Pb, some electron density from Pb is directed towards O on the $[BO_3]^{3-}$ groups. More interestingly, these interatomic interactions between the $[BO_3]^{3-}$ groups and Pb are very nicely visualized on two other planes sliced perpendicular to the *b* axis. Figure 5 c illustrates the plane with $y = 0.137$ where two O atoms in the $[BO_3]^{3-}$ group are included. This ELF diagram clearly shows the interatomic interactions between the $[BO_3]^{3-}$ trigonal-planar groups and Pb atoms, forming the extended 2D layered structures, and, as already discussed for the PDOS curves, the nearly non-bonding states of O and the p states of Pb contributing to region 4 in the PDOS curve were attributed to these interactions. Another slice with $y = 0.274$ (Figure 5 d), which is located at the midpoint between O and Pb atoms, displays comparatively weaker but still strong interatomic interactions between Pb and Cl along the *c* axis. Therefore, we claim that the interconnection of $[BO_3]^{3-}$ groups by Pb^{2+} cations in the *ab* plane results in extended 2D layers (see Figure 5 c). Furthermore, considerable interactions between lone pairs on Pb^{2+} in the 2D layers and Cl^- were observed (Figure 5 d). For comparison, an ELF diagram of the (1 −1 0) slice of KBBF was also plotted after careful theoretical calculations (Figure 5 e). No particular interactions between K and O were observed in the ELF diagram of KBBF, which may be due to an extended interatomic distance of 4.036 Å. Despite the shorter bond lengths of Be–O (1.636 Å) and F–O (2.596 Å) in KBBF compared to those of Pb–O and Cl–O in Pb_2BO_3Cl, respectively, no substantial interatomic interactions were observed between Be and O or F and O. Thus the overall networking of all of the polarizable components in the crystal structure of Pb_2BO_3Cl synergistically influences and produces a very strong SHG response. Whereas the spatial density for the $[BO_3]^{3-}$ groups in Pb_2BO_3Cl (0.00742 per unit volume) is smaller than that of KBBF (0.00946 per unit volume), the synergistic effect of the interactions between the lone pairs on the Pb^{2+} cations and Cl^- anions, and the p–π interactions between Pb^{2+} and $[BO_3]^{3-}$ groups within the extended $[Pb_2(BO_3)]^+$ layers, resulted in a very large SHG response.

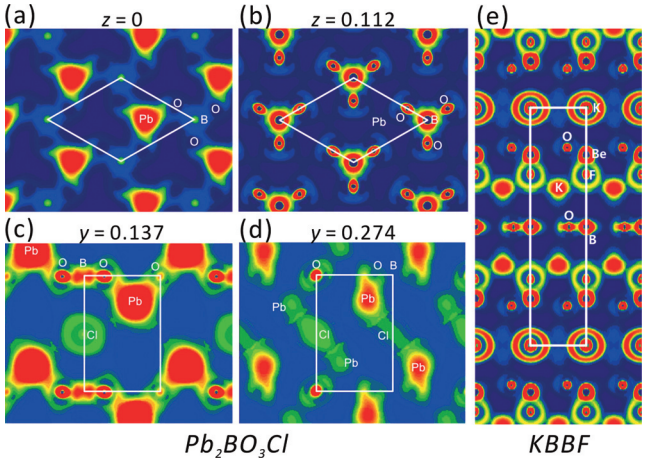

Figure 5. ELF diagrams illustrating slices along the *ab* plane with a) $z = 0$ and b) $z = 0.112$ and slices perpendicular to the *b* axis with c) $y = 0.137$ and d) $y = 0.274$ for Pb_2BO_3Cl. e) ELF diagram displaying a slice along the [0 −1 1] direction for KBBF.

Linear optical analysis shows that the refractive index dispersion curves display strong anisotropy and follow the order of $n_o > n_e$, indicating that Pb_2BO_3Cl is a uniaxial negative crystal (see Figure S4 a). The birefringence Δn is relatively large (0.12 at 1064 nm), which is favorable for phase matching in the SHG process. Compared with KBBF, the enlarged birefringence Δn, which is due to the introduction of Pb^{2+} cations, can generate strong electronic anisotropic polarizability and a large SHG response, which is also consistent with the experimental observations. As the space group of Pb_2BO_3Cl belongs to class 32 under the restrictions of Kleinman symmetry, only one set of independent SHG tensor components (d_{11}) remains. The calculated frequency-dependent SHG tensor components of Pb_2BO_3Cl are plotted in Figure S4 b. The value of d_{11} for Pb_2BO_3Cl at a wavelength of 1064 nm (1.165 eV) is 7.2 pm V^{-1}, which is slightly higher than our experimental value.

In summary, we have synthesized a new NLO material, Pb_2BO_3Cl, through a molecular engineering design approach. The material revealed a remarkably strong SHG response that was approximately nine times stronger than that of KDP, constituting the largest value ever reported for the KBBF family. A subtle balance was successfully achieved between large non-linear coefficients, moderate birefringence, and wide transparency, which means that Pb_2BO_3Cl may have great potential as a high-performance NLO material in photonic applications. The growth of large crystals for further physical property studies is ongoing. The tailored synthetic approach based on excellent crystal structures provides an opportunity to further design other structure-driven functional materials.

Acknowledgements

This research was supported by the National Research Foundation of Korea (NRF), which is funded by the Ministry of Science, ICT, and Future Planning (MSIP; 2014M3A9B8023478, 2015R1A1A1A05027845, and 2016R1A2A2A05005298). G.Z. and C.L. thank the National Natural Science Foundation of China (21401178 and 21501161).

Keywords: crystal engineering · lead borate chloride · nonlinear optical properties · second harmonic generation · X-ray diffraction

How to cite: *Angew. Chem. Int. Ed.* **2016**, *55*, 12078–12082
Angew. Chem. **2016**, *128*, 12257–12261

[1] a) K. M. Ok, P. S. Halasyamani, *Angew. Chem. Int. Ed.* **2004**, *43*, 5489–5491; *Angew. Chem.* **2004**, *116*, 5605–5607; b) S. Pan, J. P. Smit, B. Watkins, M. R. Marvel, C. L. Stern, K. R. Poeppelmeier, *J. Am. Chem. Soc.* **2006**, *128*, 11631–11634; c) K. M. Ok, E. O. Chi, P. S. Halasyamani, *Chem. Soc. Rev.* **2006**, *35*, 710–717; d) T. K. Bera, J.-H. Song, A. J. Freeman, J. I. Jang, J. B. Ketterson, M. G. Kanatzidis, *Angew. Chem. Int. Ed.* **2008**, *47*, 7828–7832; *Angew. Chem.* **2008**, *120*, 7946–7950; e) R. K. Li, P. Chen, *Inorg. Chem.* **2010**, *49*, 1561–1565; f) C.-F. Sun, C.-L. Hu, X. Xu, B.-P. Yang, J.-G. Mao, *J. Am. Chem. Soc.* **2011**, *133*, 5561–5572; g) P. Yu, L.-M. Wu, L.-J. Zhou, L. Chen, *J. Am. Chem. Soc.* **2014**, *136*, 480–487; h) S. Zhao, P. Gong, S. Luo, L. Bai, Z. Lin, Y. Tang, Y. Zhou, M. Hong, J. Luo, *Angew. Chem. Int. Ed.* **2015**, *54*, 4217–4221; *Angew. Chem.* **2015**, *127*, 4291–4295; i) H. Yu, W. Zhang, J. Young, J. M. Rondinelli, P. S. Halasyamani, *Adv. Mater.* **2015**, *27*, 7380–7385.

[2] a) S. Jin, G. Cai, W. Wang, M. He, S. Wang, X. Chen, *Angew. Chem. Int. Ed.* **2010**, *49*, 4967–4970; *Angew. Chem.* **2010**, *122*, 5087–5090; b) H. P. Wu, S. L. Pan, K. R. Poeppelmeier, H. Y. Li, D. Z. Jia, Z. H. Chen, X. Y. Fan, Y. Yang, J. M. Rondinelli, H. S. Luo, *J. Am. Chem. Soc.* **2011**, *133*, 7786–7790; c) Y. Shi, S. Pan, X. Dong, Y. Wang, M. Zhang, F. Zhang, Z. Zhou, *Inorg. Chem.* **2012**, *51*, 10870–10875; d) H. Wu, H. Yu, S. Pan, Z. Huang, Z. Yang, X. Su, K. R. Poeppelmeier, *Angew. Chem. Int. Ed.* **2013**, *52*, 3406–3410; *Angew. Chem.* **2013**, *125*, 3490–3494; e) X. Xu, C.-L. Hu, F. Kong, J.-H. Zhang, J.-G. Mao, J. Sun, *Inorg. Chem.* **2013**, *52*, 5831–5837; f) G. H. Zou, L. Huang, N. Ye, C. S. Lin, W. D. Cheng, H. Huang, *J. Am. Chem. Soc.* **2013**, *135*, 18560–18566; g) X. Fan, L. Zang, M. Zhang, H. Qiu, Z. Wang, J. Yin, H. Jia, S. Pan, C. Wang, *Chem. Mater.* **2014**, *26*, 3169–3174; h) J.-L. Song, C.-L. Hu, X. Xu, F. Kong, J.-G. Mao, *Angew. Chem. Int. Ed.* **2015**, *54*, 3679–3682; *Angew. Chem.* **2015**, *127*, 3750–3753; i) T. T. Tran, J. He, J. M. Rondinelli, P. S. Halasyamani, *J. Am. Chem. Soc.* **2015**, *137*, 10504–10507.

[3] a) R. E. Sykora, K. M. Ok, P. S. Halasyamani, T. E. Albrecht-Schmitt, *J. Am. Chem. Soc.* **2002**, *124*, 1951–1957; b) H.-S. Ra, K. M. Ok, P. S. Halasyamani, *J. Am. Chem. Soc.* **2003**, *125*, 7764–7765; c) E. O. Chi, K. M. Ok, Y. Porter, P. S. Halasyamani, *Chem. Mater.* **2006**, *18*, 2070–2074; d) C.-F. Sun, C.-L. Hu, X. Xu, J.-B. Ling, T. Hu, F. Kong, X.-F. Long, J.-G. Mao, *J. Am. Chem. Soc.* **2009**, *131*, 9486–9487; e) S. D. Nguyen, J. Yeon, S.-H. Kim, P. S. Halasyamani, *J. Am. Chem. Soc.* **2011**, *133*, 12422–12425; f) S.-J. Oh, D. W. Lee, K. M. Ok, *Inorg. Chem.* **2012**, *51*, 5393–5399; g) H. G. Kim, T. T. Tran, W. Choi, T.-S. You, P. S. Halasyamani, K. M. Ok, *Chem. Mater.* **2016**, *28*, 2424–2432.

[4] a) W.-L. Zhang, W.-D. Cheng, H. Zhang, L. Geng, C.-S. Lin, Z.-Z. He, *J. Am. Chem. Soc.* **2010**, *132*, 1508–1509; b) G. H. Zou, Z. J. Ma, K. C. Wu, N. Ye, *J. Mater. Chem.* **2012**, *22*, 19911–19918; c) H. Jo, K. M. Ok, *Inorg. Chem.* **2016**, *55*, 6286–6293.

[5] C. Chen, Y. Wu, R. Li, *Int. Rev. Phys. Chem.* **1989**, *8*, 65–91.

[6] a) P. Becker, *Adv. Mater.* **1998**, *10*, 979–992; b) S. Zhao, P. Gong, L. Bai, X. Xu, S. Zhang, Z. Sun, Z. Lin, M. Hong, C. Chen, J. Luo, *Nat. Commun.* **2014**, *5*, 4019; c) Y. Wang, S. Pan, *Coord. Chem. Rev.* **2016**, DOI: 10.1016/j.ccr.2015.12.008.

[7] C. T. Chen, B. C. Wu, A. D. Jiang, *Sci. Sin. Ser. B (Engl. Ed.)* **1985**, *28*, 235–243.

[8] C. Chen, Y. Wu, A. Jiang, B. Wu, G. You, R. Li, S. Lin, *J. Opt. Soc. Am. B* **1989**, *6*, 616–621.

[9] Y. Wu, T. Sasaki, S. Nakai, A. Yokotani, H. Tang, C. Chen, *Appl. Phys. Lett.* **1993**, *62*, 2614–2615.

[10] a) J.-M. Tu, D. A. Keszler, *Mater. Res. Bull.* **1995**, *30*, 209–215; b) Y. Mori, I. Kuroda, S. Nakajima, T. Sasaki, S. Nakai, *Appl. Phys. Lett.* **1995**, *67*, 1818–1820.

[11] M. Iwai, T. Kobayashi, H. Furuya, Y. Mori, T. Sasaki, *Jpn. J. Appl. Phys.* **1997**, *36*, L276.

[12] a) L. Mei, Y. Wang, C. Chen, B. Wu, *J. Appl. Phys.* **1993**, *74*, 7014–7015; b) D. Cyranoski, *Nature* **2009**, *457*, 953–955.

[13] S. C. Wang, N. Ye, W. Li, D. Zhao, *J. Am. Chem. Soc.* **2010**, *132*, 8779–8786.

[14] S. C. Wang, N. Ye, *J. Am. Chem. Soc.* **2011**, *133*, 11458–11461.

[15] H. Huang, J. Yao, Z. Lin, X. Wang, R. He, W. Yao, N. Zhai, C. Chen, *Angew. Chem. Int. Ed.* **2011**, *50*, 9141–9144; *Angew. Chem.* **2011**, *123*, 9307–9310.

[16] H. Huang, J. Yao, Z. Lin, X. Wang, R. He, W. Yao, N. Zhai, C. Chen, *Chem. Mater.* **2011**, *23*, 5457–5463.

[17] H. W. Yu, H. P. Wu, S. L. Pan, Z. H. Yang, X. L. Hou, X. Su, Q. Jing, K. R. Poeppelmeier, J. M. Rondinelli, *J. Am. Chem. Soc.* **2014**, *136*, 1264–1267.

[18] a) Y.-Z. Huang, L.-M. Wu, X.-T. Wu, L.-H. Li, L. Chen, Y.-F. Zhang, *J. Am. Chem. Soc.* **2010**, *132*, 12788–12789; b) X. Dong, Q. Jing, Y. Shi, Z. Yang, S. Pan, K. R. Poeppelmeier, J. Young, J. M. Rondinelli, *J. Am. Chem. Soc.* **2015**, *137*, 9417–9422; c) L. Liu, B. Zhang, F. Zhang, S. Pan, F. Zhang, X. Zhang, X. Dong, Z. Yang, *Dalton Trans.* **2015**, *44*, 7041–7047.

[19] a) I. D. Brown, D. Altermatt, *Acta Crystallogr. Sect. B* **1985**, *41*, 244–247; b) N. E. Brese, M. O'Keeffe, *Acta Crystallogr. Sect. B* **1991**, *47*, 192–197.

[20] a) W. Zhao, S. Pan, J. Han, J. Yao, Y. Yang, J. Li, M. Zhang, L. H. Zhang, Y. Hang, *J. Solid State Chem.* **2011**, *184*, 2849–2853; b) M. S. Refat, K. M. Elsabawy, *Bull. Mater. Sci.* **2011**, *34*, 873–881; c) T. T. Tran, P. S. Halasyamani, J. M. Rondinelli, *Inorg. Chem.* **2014**, *53*, 6241–6251.

[21] a) P. Kubelka, F. Munk, *Z. Tech. Phys.* **1931**, *12*, 593–601; b) J. Tauc, *Mater. Res. Bull.* **1970**, *5*, 721–729.

[22] S. Kurtz, T. Perry, *J. Appl. Phys.* **1968**, *39*, 3798–3813.

[23] a) H. Mizoguchi, H. W. Eng, P. Woodward, *Inorg. Chem.* **2004**, *43*, 1667–1680; b) H. Mizoguchi, P. Woodward, *Chem. Mater.* **2004**, *16*, 5233–5248.

Received: July 13, 2016
Revised: August 3, 2016
Published online: August 24, 2016

